ISSN 0915-633X
NIFS—217
JP9310193

Particle Orbit Analysis for LHD Helical Axis Configurations

J. Guasp, K. Yamazaki and O. Motojima

(Received – Mar. 11, 1993)

NIFS-217 Apr. 1993

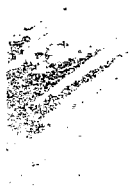

Particle Orbit Analysis for LHD Helical Axis Configurations

J. Guasp [1], K. Yamazaki, O. Motojima

National Institute for Fusion Science,
Chikusa-ku, Nagoya 464-01, Japan

[1] On leave from Asociación EURATOM / CIEMAT para Fusión. Madrid (Spain).

ABSTRACT

Fast ion orbits for helical magnetic axis configurations in LHD (Large Helical Device) are analyzed and compared with the standard circular axis case. Boundaries between passing and helically trapped particle regions show clear differences: in the non-planar axis case the helically trapped region spreads, near the magnetic axis, over a much wider band across the 90° pitch angle value and shows a very marked asymmetry. The locally trapped particle region is also wider than in the standard case. The differences in the loss cone boundaries of the two cases are rather small, however, the effects of re-entering criteria are very important in both cases. On the contrary, effects of finite coil size are not significant.

key words:
particle orbit, helically trapped particle, helical axis configuration,
loss cone, Large Helical Device.

ACKNOWLEDGEMENTS

One of the authors (J.G.) wishes to express his gratitude to the NIFS (National Institute for Fusion Science) for allowing him the opportunity to work there for several months and to know the Japanese fusion activities, and particularly to Profs. O. Motojima, K. Yamazaki and all other members of the Research Operations Division, Department of Large Helical Design Project for their polite hospitality.

Index

1. INTRODUCTION.

This study analyzes fast ion orbits in peculiar configurations of LHD (Large Helical Device) [1] where the magnetic axis has a non-circular, non-planar shape but is a spatially helical curve, and compares them with the standard case with almost complete circular axis.

These helical axis configurations (HAC) have attracted special interest not only because of the theoretical possibility, not yet tested experimentally, to attain relatively high equilibrium β limits, but also mainly for the added complexity of the magnetic ripple structure that is expected to modify strongly any orbit-related properties: losses, electric fields, wall deposition patterns, etc.

As will be shown later (in Chapter 2) LHD helical axis configurations present a medium degree of helicity, not reaching the levels of other devices (Wendelstein VII-X or TJ-II) but significant enough to expect some differences in orbit behaviors. As a natural extension of this work it is planned to use the same methods to analyze NBI particle orbits in the TJ-II device (now under construction) [2], where helicity is very high.

2. CONFIGURATIONS ANALYZED.

Three configurations have been analyzed whose electrical current settings and magnetic axis position relative to the coil center at $\phi = 0°$ appear in Table I.

The first one is the helical axis configuration (HAC) with filamentary coils, the main object of the present study. The second one, that provides for comparison, is the standard filamentary-coil LHD configuration with circular magnetic axis configuration (CAC). Schematic top and lateral views of the coils appear at Fig. 1; the major radius is 3.9 m, while the coil minor radius is 0.99 m. The third configuration analyzed corresponds to the former HAC but simulating finite-sized l=2 helical coils by means of 5 filaments for each one. The main resulting parameters appear in Table II.

As can be appraised from Table I, in the HAC case the two helical coils carry different electrical currents, in a ratio of 1 : 2, this coil current unbalance implies that the real periodicity of HAC is 5 instead of 10 as in the standard CAC. The horizontal and vertical magnetic axis excursions σ and π , in units of the major radius value and defined as:

$$\sigma \equiv \frac{\mathrm{Max}_{\forall \phi}\{R_{axis}\} - \mathrm{Min}_{\forall \phi}\{R_{axis}\}}{2 \times \mathrm{Average}_{\forall \phi}\{R_{axis}\}}$$

$$\pi \equiv \frac{\mathrm{Max}_{\forall \phi}\{Z_{axis}\}}{\mathrm{Average}_{\forall \phi}\{R_{axis}\}}$$

are shown in the last two rows of Table II. The CAC has an almost circular magnetic axis (excursions on the order of $\pm 5.10^{-4}$) while those of the HAC are around ±4%. These helicities are compared with the corresponding to other devices in Table III, it shows that the HAC of LHD have a moderate helicity and are, as has been already stated, an intermediate case between the extreme cases like Wendelstein VII-X (around ±7%) and TJ-II (±15%).

The magnetic surface cross-sections for filamentary HAC and CAC at four equally spaced toroidal angles are shown in Figs. 2 and 3. The differences are very marked in shape as well as in size. The axis excursion limits the average plasma radius in the HAC (0.43 m, while 0.56 m for the CAC), and the roughly elliptical trajectory of the magnetic axis can be seen clearly in the first one.

Another important difference is the value of the magnetic ripple on axis (Table II); very low (10^{-3}) for CAC but significant (3.2%) for the HAC, which may give an important impact upon the orbit behavior.

3. METHOD OF CALCULATION.

In this study the orbits of 10 keV protons have been calculated using a modification of the HSD vacuum field line code [3] under the Guiding Center approximation [4,5,6] and using real space coordinates, therefore no flux coordinates have been considered here. The starting points of the orbits are placed on either side along a horizontal line that intercepts the magnetic axis at a suitable toroidal angle where the helical coils are roughly in a vertical position (18°, one fourth of HAC period, see upper left plot in Figs. 2 and upper right in Fig. 3). From there the particles are launched with different pitch angles, and followed in small spatial steps until either they became lost or during around 6 characteristic drift times.

As has been demonstrated in Heliotron-E experiment [7] the effects of "re-entering", that is the possibility for a particle to leave the plasma border and come back to it later without hitting the wall, are very important. For this reason a careful attention has been given here to implement that possibility.

The main loss criterion chosen in this study is an intermediate compromise between the two extreme possibilities, namely: "no re-entering", meaning that any particle leaving the plasma border is considered immediately lost, and "total re-entering", that is, particles are considered lost only when hit the wall.

The criterion adopted here, that we call "partial re-entering", is that a particle is considered lost either when it hits the wall or when the particle distance to the magnetic axis is greater than a given value, RGLIM, that is taken as the maximum distance from the last closed magnetic surface to the magnetic axis for any toroidal angle ϕ. That is:

$$RGLIM \equiv \underset{\forall\phi}{\text{Max}} \{ \text{Distance from last magnetic surface to Magnetic Axis} \}$$

This compromise between both extremes seems less conservative and more realistic that the no reentering criterion and in the other hand tries to provide for effects like charge exchange events with the cold neutral background population that restrict the total reentering and are difficult to include in the present code.

Nevertheless the three criteria have been taken in account for the loss cone calculations (cf. §6), the difficulty to take account of reentering effects in flux coordinates, that needs to deal with the region outside the last closed magnetic surface, a region where flux coordinates properly do not exist, induced us to remain on real space coordinates.

As the main aim of this study relates to physical behavior, a simplified fictional "wall" , much more easy to handle than the complex internal helical shape of the real LHD vacuum vessel, has been considered. It consists of a simple circle centered at the coil center. The radius of this circle is 0.96 m, which corresponds to the average LHD finite coil minor radius.

Another problem that arises in helical axis configurations is the fact that the movement of the magnetic axis position across the meridian plane when toroidal angle changes (it follows an approximately elliptical path) distorts the orbit shape, that becomes rather confusing. For this reason it is convenient to eliminate this magnetic axis "drag" in order to visualize correctly the particle trajectory. This has been done here by referring the particle coordinates to the local position of the magnetic axis for each toroidal angle ϕ (coordinates R' and Z' in Fig. 4), this suppression of mgnetic axis drag is schematically represented in Fig. 4 and corresponds to the coordinate transformation $\{ R, Z \} \rightarrow \{ R', Z' \}$ the first couple being the cylindrical coordinates of the particle, the second one those referred to the local (for any fixed toroidal angle) magnetic axis position.

Finally, neither collisions nor electric field effects have been taken in account in these calculations, leaving the possibility of inclusion to future studies.

4. ORBITS.

Typical examples of the different kind of orbits are shown in Figs. 5 to 8, the regions of configuration space where each orbit type belongs are discussed in § 5.

The first one, Fig. 5, corresponds to a typical passing orbit, the starting point is placed at $x / a = +1.20$, where x is the distance to the magnetic axis and a the average plasma radius, initial pitch angle is 60°. In the figure the upper left plot represents a view of the trajectory from the top of the torus, the polar angle is the toroidal one, ϕ, the distance to the plot center the major radius. As is evident from the plot the particle turns around the torus continuously without never reversing velocity (55 turns on the plot) and without escaping.

The upper right plot of the same Figure is a "poloidal" view, that is, a projection upon the cross section of the torus. The coordinates are referred to the magnetic axis, the polar angle, in this case, is the poloidal one, θ, and the distance to the plot center the distance to magnetic axis. Obviously the particle moves spirally around the magnetic axis, circling it completely without any velocity reversal.

In both plots magnetic axis "drag" has been suppressed, as explained in § 3.

The lower left plot is a Poincaré diagram of the orbit, it is a "poloidal" view that represents, as circles, the consecutive points of

intersection between the trajectory and the $\phi = 18°$ plane (the starting point plane). As comparison, the magnetic surface cross section corresponding to the starting point is also plotted as dots. As can be seen the separation between orbit and magnetic surface is very slight in this case, at most 3 cm (less than 1% of the major radius), this is a fact common to all passing confined orbits analyzed.

The lower right plot is a similar Poincaré diagram for toroidal angle 54° (half a HAC period farther).

A typical helically trapped particle trajectory is shown in the next Fig. 6, with the same conventions that the previous one. This time the starting point is placed at $x / a = +1.20$, the same as before, but initial pitch angle is exactly 90°. In this case the particle spans only a limited arc in the toroidal direction (about 126°) reversing velocity at the extreme turning points, bouncing constantly between them (about 26 bouncings shown in the plot), it spans also a limited arc in poloidal angle (around 84°) bouncing up and down incessantly.

The corresponding Poincaré plots show the consecutive passings of the particle shifting to the inside of the initial magnetic surface and coming back to it periodically. In these cases orbit excursions are greater than for passing particles but remain yet on the order of a few cm.

Fig. 7, shows a locally trapped particle (starting point $x / a = +0.2$, initial pitch angle 90°), the particle remains trapped inside the local magnetic mirrors of two neighbor helical coil stretches (toroidal angle

span around 64°, 12 bouncings) and probably drifting extremely slowly to the inside of the torus.

Finally Fig. 8 shows the trajectory of a passing particle (starting point at $x / a = +1.30$, initial pitch angle = 60°) that should be lost under the "partial reentering" criterion but not when the "total reentering" one is used. It can be seen very clear how the orbit "sticks" to a peripheral magnetic island.

Qualitative behavior of orbits is entirely similar for the other two configurations.

5. TRAPPED PARTICLE REGIONS.

The location of the different trapping regimes: passing, helically and locally trapped particles in configuration space is represented at Figs. 9 and 10. On both diagrams the horizontal coordinate (x / a) corresponds to the starting position of the particle with respect to the magnetic axis in units of average plasma radius. The vertical coordinate is the initial pitch angle in degrees.

Fig. 9 is the diagram for the HAC while Fig. 10 corresponds to the CAC, the standard circular case. As expected, in both cases trapped particle regions cluster around the 90° pitch angle value (central horizontal line) but the differences between both cases are striking.

HAC shows a much wider angular spread in the proximities of the magnetic axis, while in the CAC case this region becomes extremely narrow spreading only across a small band (less than 2° at the axis). The obvious reason is the significant difference in magnetic ripple on this region between both configurations (cf. §2, Table II), the helical axis excursion give rise to a supplementary magnetic ripple that is almost absent in the circular case, originating more trapping opportunities. This difference smears out for greater average radius and turns, once more, to be significant on the outer part of CAC in reason of the greater size of plasma in this configuration (cf. 1st row in Table II), reversing the trend.

For the same reasons the locally trapped particle region, that in both cases is concentrated along a very narrow band across pitch angle equal 90° near the magnetic axis, is relatively wider in the HAC case and extends not only to the inside of the torus, like in CAC, but also, partially, to the outside, although it remains small.

Another important fact of the HAC is the existence of very clear asymmetry around pitch angle 90°, which comes directly from the difference in electrical currents between the two l=2 helical coils that is absent in the CAC case (cf. Table I).

6. LOSS CONE DIAGRAM.

Figures 11 and 12 show the loss cone structure in configuration space (initial position and pitch angle) for both HAC and CAC cases. These plots have the same coordinate system that those of Figs. 9 and 10. The differences between both configurations are visible but not very important, the characteristic indentations towards the plasma interior that appear usually at the boundary between passing and helically trapped particle regions are visible, but located at different positions because plasma radius is greater for CAC, and in both cases are not very pronounced.

On the other hand the influence of the different reentering criteria is extremely clear in both cases reflecting the same facts as in Heliotron-E experiment [7] and stressing the importance of a good modeling of the peripheral region: magnetic structure, neutral background and real shape of limiters and vacuum vessel, difficult points that may eliminate the advantages of a calculation in magnetic flux coordinates where these loss criteria are difficult to handle.

7. FINITE-SIZED COIL EFFECTS.

In order to observe the influence of finite size coils, the third configuration analyzed is identical to the previous HAC bur each one of the two helical coils have been modeled with 5 filaments. The coil structure appears schematically, as top and lateral view, in Fig. 13 (that must be compared with Fig. 1), and the magnetic surface cross sections at Fig. 14. As can be seen there is no qualitative difference between both cases (see also Fig. 2 and Table II).

This lack of significant differences implies that the orbits are also qualitatively similar. Fig. 15 compares the boundaries between the different trapped regions for both cases, the finite coil case is represented by triangles (helically trapped/passing boundary) and small circles (locally trapped), while the filamentary HAC case is represented by continuous lines. Only near the plasma border, where the finiteness of the coils modifies the magnetic field structure, the differences are sensible.

This difference is also small for the loss cone structure in configuration space, as shows Fig. 16 , where continuous lines correspond, this time, to the finite coil case and dashed ones to the filamentary one.

8. CONCLUSIONS

In conclusion: strong differences appear between Helical Axis Configuration (HAC) and the standard circular one (CAC)

HAC shows wider spreading of the helically trapped region around the 90° pitch angle value.

The concentration of locally trapped particles around a narrow region across 90° and near the magnetic axis, preferentially on the inner side, is less pronounced for the HAC where those particles spread around a wider and longer band.

Both effects are to be related to the different magnetic ripple structure, the helical axis excursion giving rise to more trapping opportunities in the HAC case.

There exist a very marked asymmetry around 90° for HAC.

The effect of re-entering upon the loss cone structure are very pronounced in both cases.

And, finally, there appears only a small influence of finite coil effects.

Intended future extensions of this study will apply these calculations to a more pronounced helical configuration, like the corresponding to TJ-II device, for its NBI analysis and will compare the results of real space and flux coordinate codes for both devices. Inclusion of collisions and electric field effects is also planned.

9. REFERENCES

[1]. IIYOSHI,A., FUJIWARA,M., MOTOJIMA,O., OHYABU,N., YAMAZAKI,K., Fusion Tech. **17** (1990) 169.

[2]. *TJ-II* DESIGN GROUP, Fusion Tech. **17** (1990) 131.

[3]. YAMAZAKI,K., HSD code, private communication (1992).

[4]. MIYAMOTO,K., "Plasma Physics for Nuclear Fusion". MIT Press, 1980.

[5]. ABE,Y., MATSUOKA,K., SATO,M., MIYAMOTO,K., Institute of Plasma Physics, Nagoya University Report IPPJ-397 (1979).

[6]. SANUKI,H., TODOROKI,J., KAMIMURA,T., National Institute for Fusion Science Research Report NIFS-9 (1990).

[7]. HANATANI,K., NAKASHIMA,Y., ZUSHI,H., SANO,F., MOTOJIMA,O., WAKATANI,M., OBIKI,T., IIYOSHI,A., UO,K., Nucl. Fusion **25** (1985) 259.

10. FIGURE CAPTIONS.

Fig. 1. Schematic top and lateral view of LHD coils (single filament).

Fig. 2. Magnetic surface cross sections for 4 toroidal angles corresponding to the helical axis configuration with filamentary coils.

Fig. 3. Ibid. for the circular axis case (filamentary coils).

Fig. 4. Coordinate transformation for magnetic axis "drag" elimination.

Fig. 5. A typical passing particle orbit example for the filamentary helical axis configuration. Magnetic axis "drag" has been adopted.
(Starting point $x / a = +1.20$, Pitch angle = 60°)

Upper left figure corresponds to a tow view of the orbit. Distance to the plot center is major radius and the polar angle is the toroidal one ϕ.

Upper right figure corresponds to a "poloidal" view of the orbit referred to the local position of magnetic axis, distance to the plot center is the distance to the magnetic axis and the polar angle is the poloidal one.

Lower left figure corresponds to a Poincare plot of the orbit showing the successive crossings at toroidal angle = 18°, the launching plane, and the starting point magnetic surface cross section.

Lower right figure is like the previous one but for a toroidal angle = 54° (half a HAC period further).

Fig. 6. As Fig. 5, but for a helically trapped particle.
(Starting point $x / a = +1.20$, Pitch angle = 90°)

Fig. 7. As Fig. 5, but for a locally trapped particle.
(Starting point $x / a = +0.20$, Pitch angle = 90°)

Fig. 8. As Fig. 5, but for a passing particle, that should be lost under the "partial" reentering criterion, but not under the "total" reentering one, showing the neighborhood of a peripheral magnetic island. (Starting point $x/a = +1.30$, Pitch angle = 60°).

Fig. 9. Boundaries between different trapped regimes for the helical axis configuration. Horizontal coordinate (x/a) is the distance from the starting point to the magnetic axis, in units of the average plasma radius. Vertical coordinate is initial pitch angle in degrees. Black squares correspond to the loss cone (cf. Fig. 11).

Fig. 10. As Fig. 9 but for the circular axis configuration.

Fig. 11. Loss cone diagram for the filamentary helical axis configuration showing the strong effect of the different reentering criteria. Same coordinates as in Fig. 9. Black circles correspond to the boundary between passing and helically trapped particles.

Fig. 12. Same as Fig. 11, but for the filamentary circular axis case.

Fig. 13. Schematic top and lateral view of LHD coils for the multiple filament helical coils (5 filaments) that simulates finite coil effects.

Fig. 14. Magnetic surface cross sections for 4 toroidal angles corresponding to the helical axis configuration with finite coils

Fig. 15. Comparison between the boundaries of the different trapped regimes for the helical axis configuration in the filamentary (continuous lines) and finite coil cases (triangles and circles). The black squares correspond to the loss cone for the filamentary case. Same coordinates as in Fig. 9.

Fig. 16. Same as Fig. 15 but showing the small differences in the loss cone diagram between the finite (continuous lines) and filamentary coil cases (dashed lines).

Table I

Current Settings for Analyzed Configurations

Currents (MA)	Circular Axis Configuration	Helical Axis Configuration (filamentary)	Helical Axis Configuration (finite coils)
Helical Coil 1	7.8	3.9	3.9
Helical Coil 2	7.8	7.8	7.8
Poloidal Coil 1	-3.86	-3.22	-3.13
Poloidal Coil 2	-2.16	-1.24	-1.23
Poloidal Coil 3	+3.73	+2.72	+2.56
Magnetic Axis Shift (m)	-0.10	-0.15	-0.15

Table II

Main Parameters for Analyzed Configurations

Parameter	Circular Axis Configuration	Helical Axis Configuration (filamentary)	Helical Axis Configuration (finite coils)
Average Radius a (m)	0.56	0.43	0.44
iota on Axis t(0)	0.46	0.59	0.47
iota at Edge t(a)	1.17	0.96	0.80
Magnetic Well Depth (%)	17.2	16.3	15.0
Average Magnetic Field on Axis (T)	4.1	3.2	3.2
Field Ripple on Axis (%)	0.1	3.7	2.9
Field Ripple at r = 0.43 m (%)	25.0	26.8	25.5
Horizontal Magnetic Axis Excursion σ (%)	±0.05	±4.0	±3.8
Vertical Magnetic Axis Excursion π (%)	±0.05	±4.4	±4.2

Table III

Degree of Non-Circularity (σ) / Non-Planarity (π) for Several Helical Axis Configurations:

Configuration	Non-Circularity (σ)	Non-Planarity (π)
LHD (Circular Axis)	$\pm 5.\ 10^{-4}$	$\pm 5.\ 10^{-4}$
LHD (Helical Axis)	± 4.0 %	± 4.4 %
TJ-I Up.	± 4.2 %	± 4.2 %
W 7-X	± 7.5 %	± 5 %
TJ-II	± 15 %	± 15 %

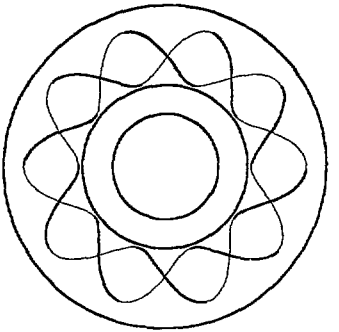

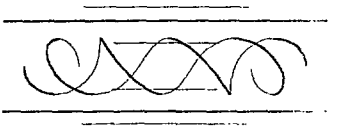

Fig. 1

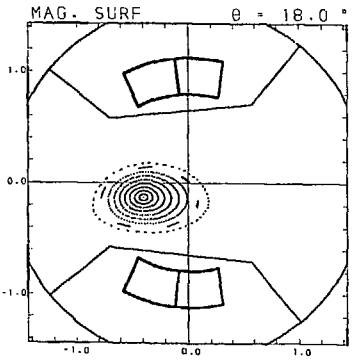

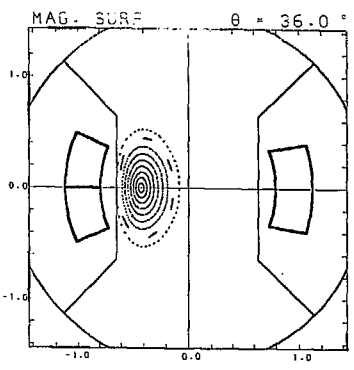

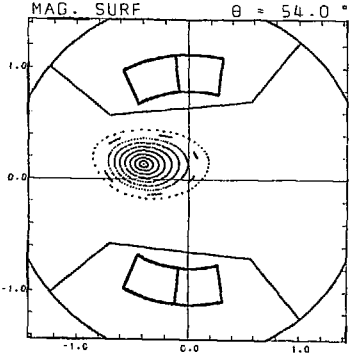

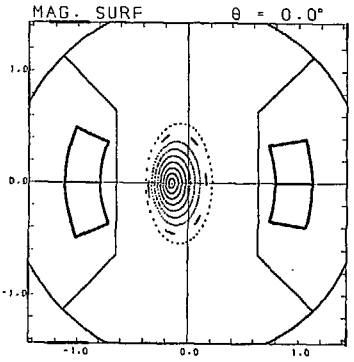

XM	= 5.000
RO	= 3.900
A	= 0.955
HEIGHT	= 0.326
WIDTH	= 0.503
ALPHA*	= 0.100
BETA*	= 0.0
AXIS	= -0.150
RX	= -0.642
PITCHO	= 1.224
CURRH	= 3.9000
(A/MM2)	= 23.8
TVA	= 0.341
WVT	= 1.543
Currp	= -3.220
Currp	= -1.241
Currp	= 2.719
CURR(I)	= 3.900
GAMMA	= 1.224

Fig. 2

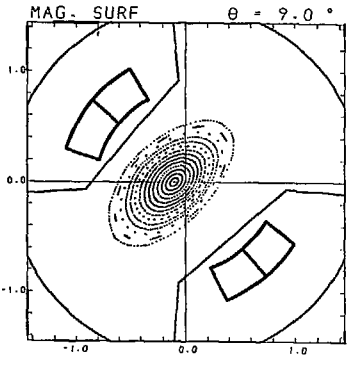

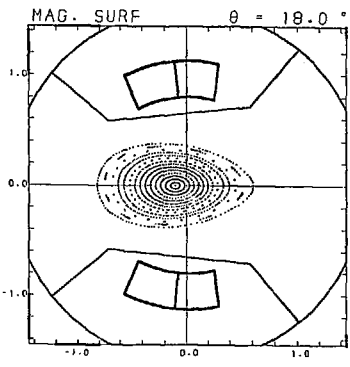

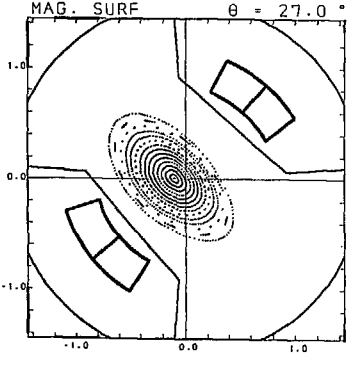

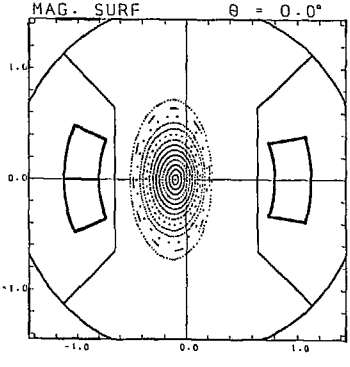

XM = 5.000
RO = 3.900
A = 0.963
HEIGHT = 0.326
WIDTH = 0.490
ALPHA* = 0.100
BETA* = 0.0
AXIS = -0.100
RX = -0.650
PITCHO = 1.235

CURRH = 7.8000
(A/MM2) = 48.8

TVA = 0.338
WVT = 1.503

Currp = -3.861
Currp = -2.163
Currp = 3.728

CURR(I) = 7.800
GAMMA = 1.235

Fig. 3

Magnetic Axis "drag" elimination in Helical Axis Configurations

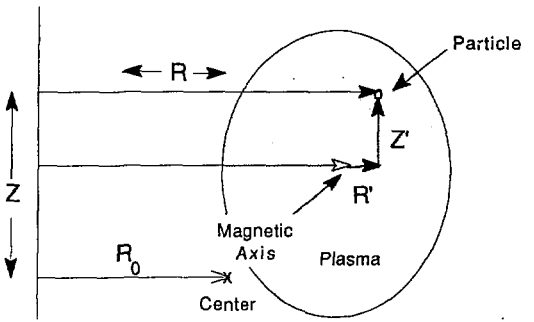

$$\{ R , Z \} \Rightarrow \{ R' , Z' \}$$

Fig. 4

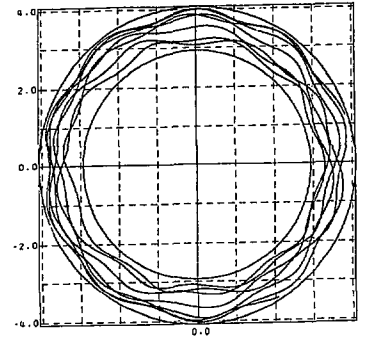
4.0
2.0
0.0
-2.0
-4.0
0.0

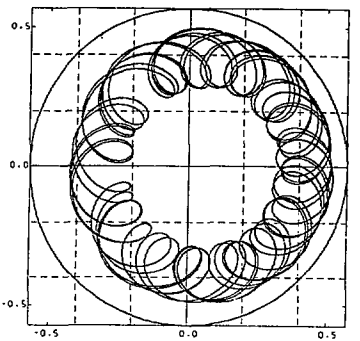
0.5
0.0
-0.5
-0.5
0.0
0.5

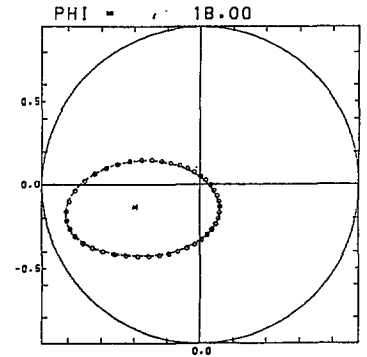
PHI = 18.00
0.5
0.0
-0.5
0.0

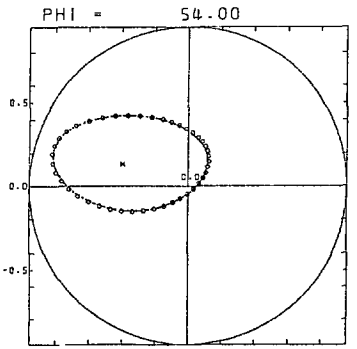
PHI = 54.00
0.5
0.0
-0.5

Fig. 5

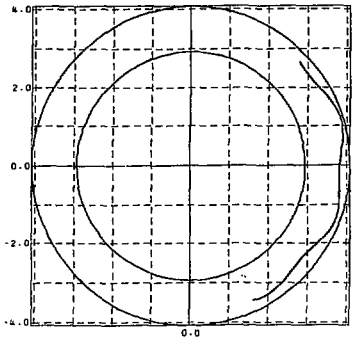
4.0
2.0
0.0
-2.0
-4.0
0.0

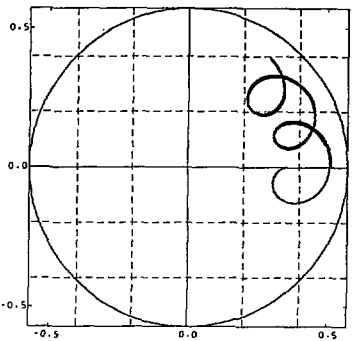
0.5
0.0
-0.5
-0.5
0.0
0.5

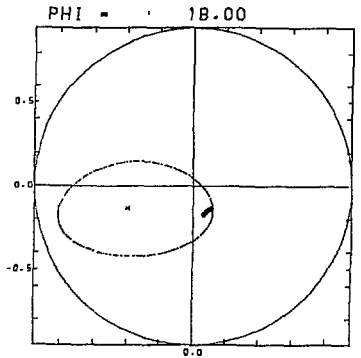
PHI = 18.00
0.5
0.0
-0.5
0.0

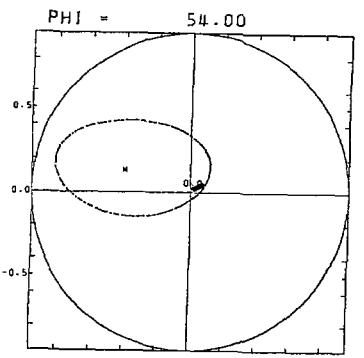
PHI = 54.00
0.5
0.0
-0.5

Fig. 6

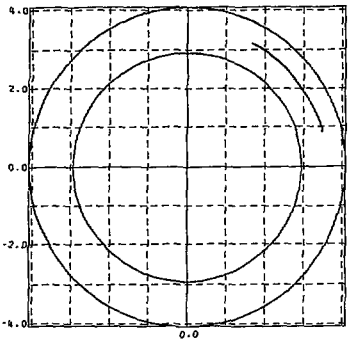
4.0
2.0
0.0
-2.0
-4.0
0.0

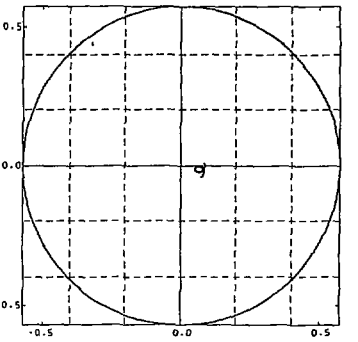
0.5
0.0
-0.5
-0.5
0.0
0.5

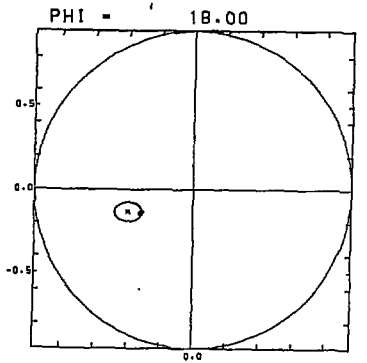
PHI = 18.00
0.5
0.0
-0.5
0.0

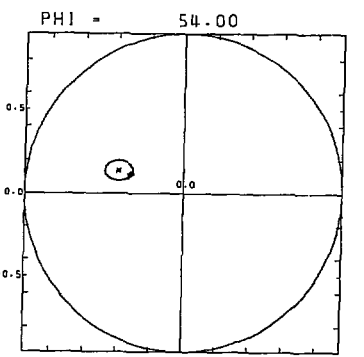
PHI = 54.00
0.5
0.0
-0.5
0.0

Fig. 7

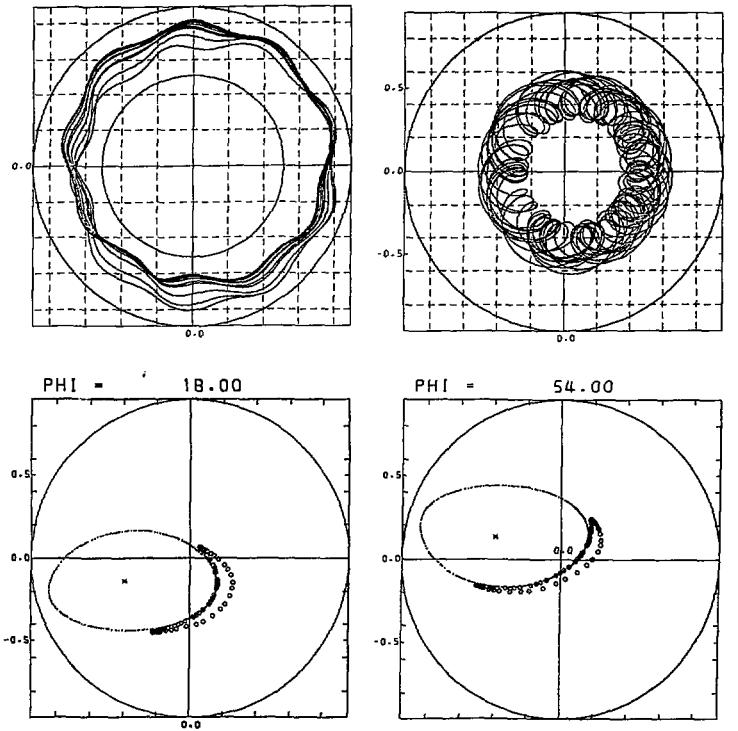

Fig. 8

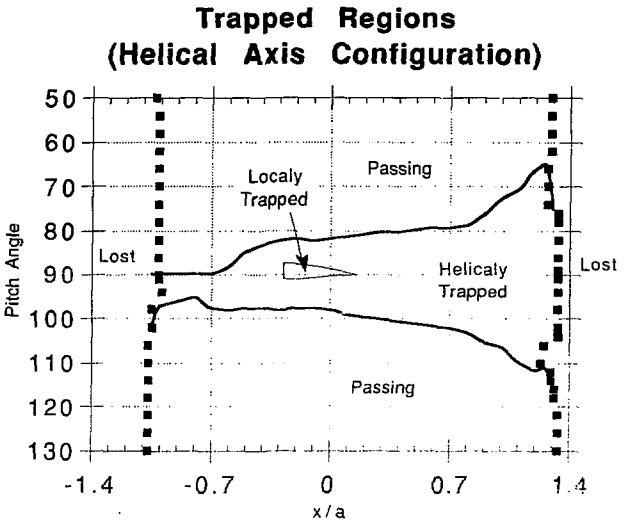
Trapped Regions
(Helical Axis Configuration)
Pitch Angle
50
60
70
80
90
100
110
120
130
-1.4
-0.7
0
0.7
1.4
x/a
Localy
Trapped
Passing
Lost
Helicaly
Trapped
Lost
Passing

Fig. 9

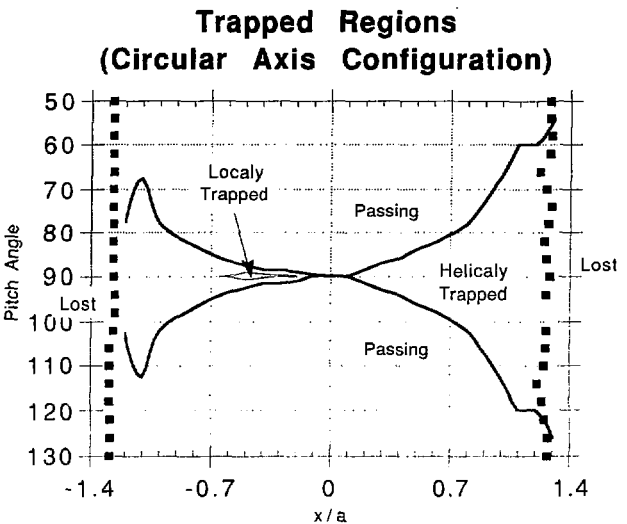
Trapped Regions
(Circular Axis Configuration)
Pitch Angle
50
60
70
80
90
100
110
120
130
Localy
Trapped
Passing
Helicaly
Trapped
Lost
Lost
Passing
-1.4
-0.7
0
0.7
1.4
x / a

Fig. 10

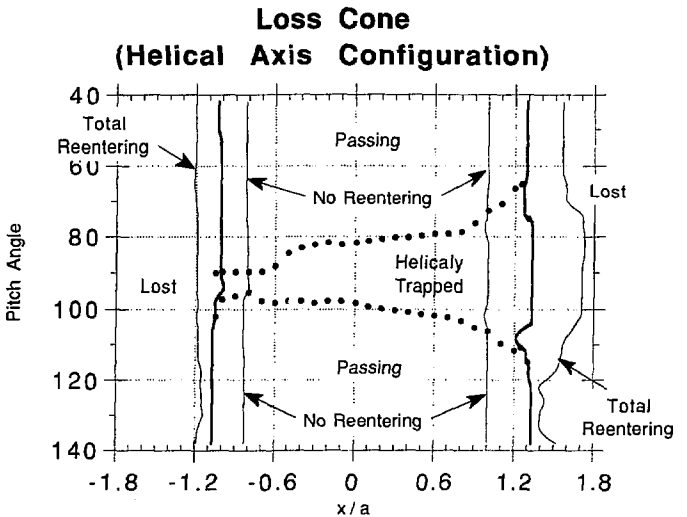
Loss Cone
(Helical Axis Configuration)
Pitch Angle
40
60
80
100
120
140
Total
Reentering
Passing
No Reentering
Lost
Helicaly
Trapped
Lost
Passing
No Reentering
Total
Reentering
-1.8
-1.2
-0.6
0
0.6
1.2
1.8
x / a

Fig. 11

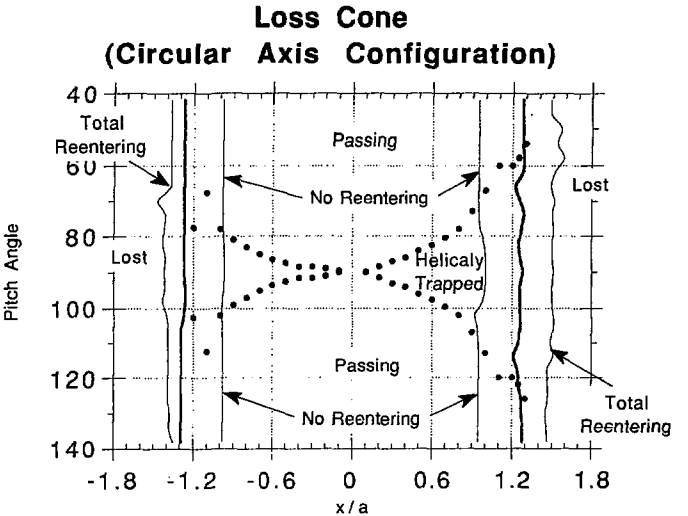
Loss Cone
(Circular Axis Configuration)
Pitch Angle
40
60
80
100
120
140
Total
Reentering
Passing
No Reentering
Lost
Helicaly
Trapped
Lost
Passing
No Reentering
Total
Reentering
-1.8
-1.2
-0.6
0
0.6
1.2
1.8
x / a

Fig. 12

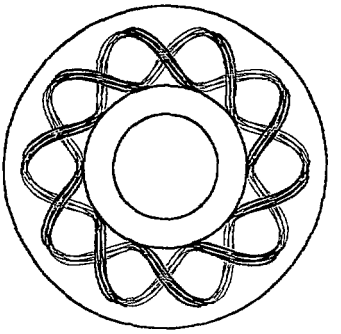

Fig. 13

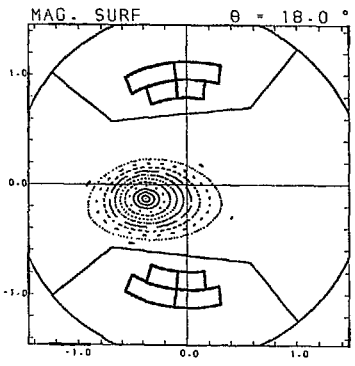

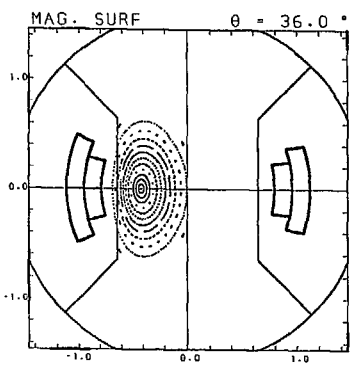

XM = 5.000
RO = 3.900
A = 0.971
HEIGHT = 0.326
WIOTH = 0.503
ALPHA* = 0.100
BETA* = 0.0
AXIS = -0.150
RX = -0.642
PITCHO = 1.224

CURRH = 3.9000
(A/MM2) = 28.5

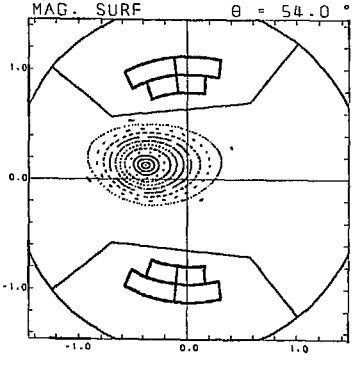

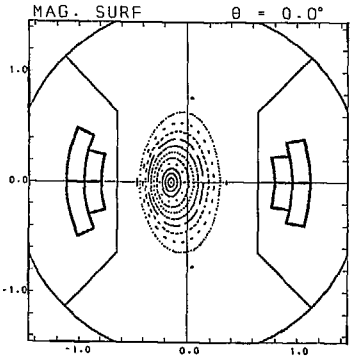

TVA = 0.341
WVT = 1.543

Currp = -3.130
Currp = -1.233
Currp = 2.560

CURR(I) = 2.340
CURR(I) = 1.560
GAMMA = 1.245

Fig. 14

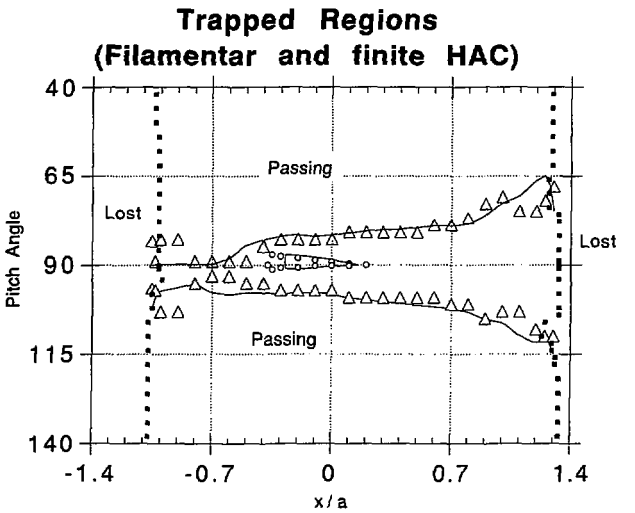
Trapped Regions
(Filamentar and finite HAC)
40
65
90
115
140
Pitch Angle
Passing
Lost
Lost
Passing
-1.4
-0.7
0
0.7
1.4
x/a

Fig. 15

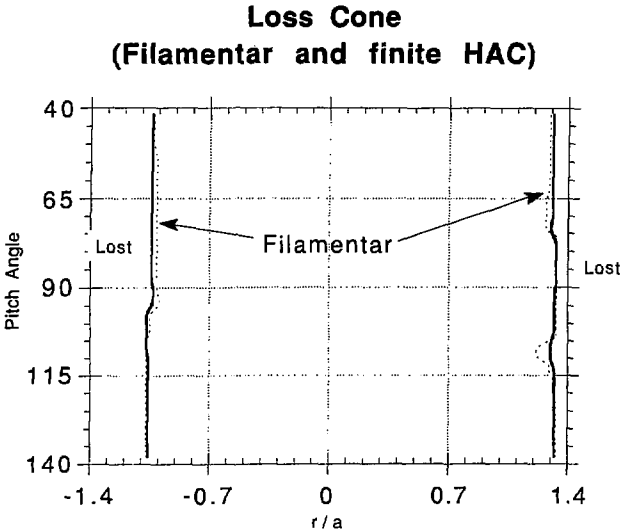
Loss Cone
(Filamentar and finite HAC)
40
65
90
115
140
Pitch Angle
Lost
Filamentar
Lost
-1.4
-0.7
0
0.7
1.4
r / a

Fig. 16

Recent Issues of NIFS Series

NIFS-173 N. Nakajima, J. Todoroki and M. Okamoto, *On Relation between Hamada and Boozer Magnetic Coordinate System* ; Sep. 1992

NIFS-174 K. Ichiguchi, N. Nakajima, M. Okamoto, Y. Nakamura and M. Wakatani, *Effects of Net Toroidal Current on Mercier Criterion in the Large Helical Device* ; Sep. 1992

NIFS-175 S. -I. Itoh, K. Itoh and A. Fukuyama, *Modelling of ELMs and Dynamic Responses of the H-Mode* ; Sep. 1992

NIFS-176 K. Itoh, S.-I. Itoh, A. Fukuyama, H. Sanuki, K. Ichiguchi and J. Todoroki, *Improved Models of β-Limit, Anomalous Transport and Radial Electric Field with Loss Cone Loss in Heliotron / Torsatron* ; Sep. 1992

NIFS-177 N. Ohyabu, K. Yamazaki, I. Katanuma, H. Ji, T. Watanabe, K. Watanabe, H. Akao, K. Akaishi, T. Ono, H. Kaneko, T. Kawamura, Y. Kubota, N. Noda, A. Sagara, O. Motojima, M. Fujiwara and A. Iiyoshi, *Design Study of LHD Helical Divertor and High Temperature Divertor Plasma Operation* ; Sep. 1992

NIFS-178 H. Sanuki, K. Itoh and S.-I. Itoh, *Selfconsistent Analysis of Radial Electric Field and Fast Ion Losses in CHS Torsatron / Heliotron* ; Sep. 1992

NIFS-179 K. Toi, S. Morita, K. Kawahata, K. Ida, T. Watari, R. Kumazawa, A. Ando, Y. Oka, K. Ohkubo, Y. Hamada, K. Adati, R. Akiyama, S. Hidekuma, S. Hirokura, O. Kaneko, T. Kawamoto, Y. Kawasumi, M. Kojima, T. Kuroda, K. Masai, K. Narihara, Y. Ogawa, S. Okajima, M. Sakamoto, M. Sasao, K. Sato, K. N. Sato, T. Seki, F. Shimpo, S. Tanahashi, Y. Taniguchi, T. Tsuzuki, *New Features of L-H Transition in Limiter H-Modes of JIPP T-IIU* ; Sep. 1992

NIFS-180 H. Momota, Y. Tomita, A. Ishida, Y. Kohzaki, M. Ohnishi, S. Ohi, Y. Nakao and M. Nishikawa, *D-^{3}He Fueled FRC Reactor "Artemis-L"* ; Sep. 1992

NIFS-181 T. Watari, R. Kumazawa, T. Seki, Y. Yasaka, A. Ando, Y. Oka,O. Kaneko, K. Adati, R. Akiyama, Y. Hamada, S. Hidekuma, S. Hirokura, K. Ida, K. Kawahata, T. Kawamoto, Y. Kawasumi, S. Kitagawa, M. Kojima, T. Kuroda, K. Masai, S. Morita, K. Narihara, Y. Ogawa, K. Ohkubo, S. Okajima, T. Ozaki, M. Sakamoto, M. Sasao, K. Sato, K. N. Sato, F.Shimpo, H. Takahashi, S. Tanahasi, Y. Taniguchi, K. Toi, T. Tsuzuki and M. Ono, *The New Features of Ion Bernstein Wave Heating in JIPP T-IIU Tokamak* ;Sep, 1992

NIFS-182 K. Itoh, H. Sanuki and S.-I. Itoh, *Effect of Alpha Particles on Radial Electric Field Structure in Torsatron / Heliotron Reactor*; Sep. 1992

NIFS-183 S. Morimoto, M. Sato, H. Yamada, H. Ji, S. Okamura, S. Kubo, O. Motojima, M. Murakami, T. C. Jernigan, T. S. Bigelow, A. C. England, R. S. Isler, J. F. Lyon, C. H. Ma, D. A. Rasmussen, C. R. Schaich, J. B. Wilgen and J. L. Yarber, *Long Pulse Discharges Sustained by Second Harmonic Electron Cyclotron Heating Using a $35GH_Z$ Gyrotron in the Advanced Toroidal Facility*; Sep. 1992

NIFS-184 S. Okamura, K. Hanatani, K. Nishimura, R. Akiyama, T. Amano, H. Arimoto, M. Fujiwara, M. Hosokawa, K. Ida, H. Idei, H. Iguchi, O. Kaneko, T. Kawamoto, S. Kubo, R. Kumazawa, K. Matsuoka, S. Morita, O. Motojima, T. Mutoh, N. Nakajima, N. Noda, M. Okamoto, T. Ozaki, A. Sagara, S. Sakakibara, H. Sanuki, T. Seki, T. Shoji, F. Shimbo, C. Takahashi, Y. Takeiri, Y. Takita, K. Toi, K. Tsumori, M. Ueda, T. Watari, H. Yamada and I. Yamada, *Heating Experiments Using Neutral Beams with Variable Injection Angle and ICRF Waves in CHS* ; Sep. 1992

NIFS-185 H. Yamada, S. Morita, K. Ida, S. Okamura, H. Iguchi, S. Sakakibara, K. Nishimura, R. Akiyama, H. Arimoto, M. Fujiwara, K. Hanatani, S. P. Hirshman, K. Ichiguchi, H. Idei, O. Kaneko, T. Kawamoto, S. Kubo, D. K. Lee, K. Matsuoka, O, Motojima, T. Ozaki, V. D. Pustovitov, A. Sagara, H. Sanuki, T. Shoji, C. Takahashi, Y. Takeiri, Y. Takita, S. Tanahashi, J. Todoroki, K. Toi, K. Tsumori, M. Ueda and I. Yamada, *MHD and Confinement Characteristics in the High-β Regime on the CHS Low-Aspect-Ratio Heliotron / Torsatron* ; Sep. 1992

NIFS-186 S. Morita, H. Yamada, H. Iguchi, K. Adati, R. Akiyama, H. Arimoto, M. Fujiwara, Y. Hamada, K. Ida, H. Idei, O. Kaneko, K. Kawahata, T. Kawamoto, S. Kubo, R. Kumazawa, K. Matsuoka, T. Morisaki, K. Nishimura, S. Okamura, T. Ozaki, T. Seki, M. Sakurai, S, Sakakibara, A. Sagara, C. Takahashi, Y. Takeiri, H. Takenaga, Y. Takita, K. Toi, K. Tsumori, K. Uchino, M. Ueda, T. Watari, I. Yamada, *A Role of Neutral Hydrogen in CHS Plasmas with Reheat and Collapse and Comparison with JIPP T-IIU Tokamak Plasmas* ; Sep. 1992

NIFS-187 K. Ioth, S.-I. Itoh, A. Fukuyama, M. Yagi and M. Azumi, *Model of the L-Mode Confinement in Tokamaks* ; Sep. 1992

NIFS-188 K. Itoh, A. Fukuyama and S.-I. Itoh, *Beta-Limiting Phenomena in High-Aspect-Ratio Toroidal Helical Plasmas*; Oct. 1992

NIFS-189 K. Itoh, S. -I. Itoh and A. Fukuyama, *Cross Field Ion Motion at Sawtooth Crash* ; Oct. 1992

NIFS-190 N. Noda, Y. Kubota, A. Sagara, N. Ohyabu, K. Akaishi, H. Ji, O. Motojima, M. Hashiba, I. Fujita, T. Hino, T. Yamashina, T. Matsuda, T. Sogabe, T. Matsumoto, K. Kuroda, S. Yamazaki, H. Ise, J. Adachi and T. Suzuki, *Design Study on Divertor Plates of Large Helical Device (LHD)* ; Oct. 1992

NIFS-191 Y. Kondoh, Y. Hosaka and K. Ishii, *Kernel Optimum Nearly-Analytical Discretization (KOND) Algorithm Applied to Parabolic and Hyperbolic Equations* : Oct. 1992

NIFS-192 K. Itoh, M. Yagi, S.-I. Itoh, A. Fukuyama and M. Azumi, *L-Mode Confinement Model Based on Transport-MHD Theory in Tokamaks* ; Oct. 1992

NIFS-193 T. Watari, *Review of Japanese Results on Heating and Current Drive* ; Oct. 1992

NIFS-194 Y. Kondoh, *Eigenfunction for Dissipative Dynamics Operator and Attractor of Dissipative Structure* ; Oct. 1992

NIFS-195 T. Watanabe, H. Oya, K. Watanabe and T. Sato, *Comprehensive Simulation Study on Local and Global Development of Auroral Arcs and Field-Aligned Potentials* ; Oct. 1992

NIFS-196 T. Mori, K. Akaishi, Y. Kubota, O. Motojima, M. Mushiaki, Y. Funato and Y. Hanaoka, *Pumping Experiment of Water on B and LaB_6 Films with Electron Beam Evaporator* ; Oct., 1992

NIFS-197 T. Kato and K. Masai, *X-ray Spectra from Hinotori Satellite and Suprathermal Electrons* ; Oct. 1992

NIFS-198 K. Toi, S. Okamura, H. Iguchi, H. Yamada, S. Morita, S. Sakakibara, K. Ida, K. Nishimura, K. Matsuoka, R. Akiyama, H. Arimoto, M. Fujiwara, M. Hosokawa, H. Idei, O. Kaneko, S. Kubo, A. Sagara, C. Takahashi, Y. Takeiri, Y. Takita, K. Tsumori, I. Yamada and H. Zushi, *Formation of H-mode Like Transport Barrier in the CHS Heliotron / Torsatron* ; Oct. 1992

NIFS-199 M. Tanaka, *A Kinetic Simulation of Low-Frequency Electromagnetic Phenomena in Inhomogeneous Plasmas of Three-Dimensions* ; Nov. 1992

NIFS-200 K. Itoh, S.-I. Itoh, H. Sanuki and A. Fukuyama, *Roles of Electric Field on Toroidal Magnetic Confinement*, Nov. 1992

NIFS-201 G. Gnudi and T. Hatori, *Hamiltonian for the Toroidal Helical Magnetic Field Lines in the Vacuum*; Nov. 1992

NIFS-202 K. Itoh, S.-I. Itoh and A. Fukuyama, *Physics of Transport Phenomena in Magnetic Confinement Plasmas*; Dec. 1992

NIFS-203 Y. Hamada, Y. Kawasumi, H. Iguchi, A. Fujisawa, Y. Abe and M. Takahashi, *Mesh Effect in a Parallel Plate Analyzer*; Dec. 1992

NIFS-204 T. Okada and H. Tazawa, *Two-Stream Instability for a Light Ion Beam -Plasma System with External Magnetic Field;* Dec. 1992

NIFS-205 M. Osakabe, S. Itoh, Y. Gotoh, M. Sasao and J. Fujita, *A Compact Neutron Counter Telescope with Thick Radiator (Cotetra) for Fusion Experiment*; Jan. 1993

NIFS-206 T. Yabe and F. Xiao, *Tracking Sharp Interface of Two Fluids by the CIP (Cubic-Interpolated Propagation) Scheme*, Jan. 1993

NIFS-207 A. Kageyama, K. Watanabe and T. Sato, *Simulation Study of MHD Dynamo : Convection in a Rotating Spherical Shell*; Feb. 1993

NIFS-208 M. Okamoto and S. Murakami, *Plasma Heating in Toroidal Systems*; Feb. 1993

NIFS-209 K. Masai, *Density Dependence of Line Intensities and Application to Plasma Diagnostics*; Feb. 1993

NIFS-210 K. Ohkubo, M. Hosokawa, S. Kubo, M. Sato, Y. Takita and T. Kuroda, *R&D of Transmission Lines for ECH System* ; Feb. 1993

NIFS-211 A. A. Shishkin, K. Y. Watanabe, K. Yamazaki, O. Motojima, D. L. Grekov, M. S. Smirnova and A. V. Zolotukhin, *Some Features of Particle Orbit Behavior in LHD Configurations*; Mar. 1993

NIFS-212 Y. Kondoh, Y. Hosaka and J.-L. Liang, *Demonstration for Novel Self-organization Theory by Three-Dimensional Magnetohydrodynamic Simulation*; Mar. 1993

NIFS-213 K. Itoh, H. Sanuki and S.-I. Itoh, *Thermal and Electric Oscillation Driven by Orbit Loss in Helical Systems*; Mar. 1993

NIFS-214 T. Yamagishi, *Effect of Continuous Eigenvalue Spectrum on Plasma Transport in Toroidal Systems*; Mar. 1993

NIFS-215 K. Ida, K. Itoh, S.-I.Itoh, Y. Miura, JFT-2M Group and A. Fukuyama, *Thickness of the Layer of Strong Radial Electric Field in JFT-2M H-mode Plasmas*; Apr. 1993

NIFS-216 M. Yagi, K. Itoh, S.-I. Itoh, A. Fukuyama and M. Azumi, *Analysis of Current Diffusive Ballooning Mode*; Apr. 1993